SUPERVISED CLASSIFICATION BY NEURAL NETWORKS USING POLARIMETRIC TIME-FREQUENCY SIGNATURES

M. Duquenoy[1,2]*, J.P. Ovarlez*[1,3]*, C. Morisseau*[1]*, G. Vieillard*[1]*, L. Ferro-Famil*[2] *and E. Pottier*[2]

[1] : ONERA, The French Aerospace lab, DEMR/TSI, Palaiseau, FRANCE,

mickael.duquenoy@gmail.com, {jean-philippe.ovarlez||christele.morisseau||gilles.vieillard}@onera.fr

[2] : IETR, Image and Remote Sensing Group, SAPHIR Team, University of Rennes 1, FRANCE

{laurent.ferro-famil||eric.pottier}@univ-rennes1.fr

[3] : SONDRA, Supélec, FRANCE

ABSTRACT

In radar imaging, the assumption is made that scatterers are white in the emitted frequency band and isotropic for all direction of observation. Nevertheless, new capacities in radar imaging, using a wideband and a large angular excursion, make these hypotheses not valid. Time-frequency analysis highlight this point of view and show some scatterers are anisotropic and/or dispersive. This information source can be completed by radar polarimetry. This paper suggests a supervised classification of scatterers using neural networks based on polarimetric time-frequency signatures. This method is applied here on anechoic chamber data, however can be generalized to SAR or circular SAR imaging.

Index Terms— Wavelet Transform, Radar Imaging, Neural Network, Target Classification

1. INTRODUCTION

Conventional radar imaging techniques consider targets as a set of bright points. Indeed, it considers scatterers as isotropic for all the directions of presentation and white in the frequency band[1], [2]. Recent studies showed, using time-frequency analysis, thee angular and frequency behavior of the spatial distribution of all image scatterers [3], [4], [5]. These representations, called hyperimages, showed that some scatterers were neither isotropic nor white. This non-stationary behavior of scatterers can be explained by their material (dispersive), their geometry (anisotropic and dispersive) or their orientation (anisotropic).

Polarimetry is another information source about the geometry and the orientation of scatterers in radar imaging. Recent studies showed, using time-frequency analysis and polarimetric coherent decompositions, the polarimetric angular and frequency behavior of the spatial distribution of all image scatterers [6]. These representations, called polarimetric hyperimages, showed that some scatterers were not polarimetric stationary.

The aim of this paper is to classify scatterers according to their energetic or polarimetric behaviors. This paper presents the construction of polarimetric time-frequency signatures. Then, the signature of canonical targets is extracted and a process of classification is designed by neural networks to discriminate data from anechoic chamber.

2. RADAR IMAGING

2.1. Classical Radar Imaging

The model usually used in radar imaging is the model of bright points [7]. The object under analysis can be seen as a set of bright points, i.e. a set of independent sources which reflect in the same way for all frequencies (white points) and all directions of presentation (isotropic points). Let $S(\mathbf{r})$ be the complex amplitude of the bright point response located at $\mathbf{r} = (x, y)^T$ in a set of cartesian axes related to the object. Under far field conditions (decomposition into planes waves), the complex backscattering coefficient for the whole object is then given by the in-phase summation of each reflector contribution:

$$H(\mathbf{k}) = \int S(\mathbf{r})\, e^{-2i\pi \mathbf{k}.\mathbf{r}}\, d\mathbf{r}. \tag{1}$$

After a Fourier Transform of (1), one can obtain the complex amplitude of spatial repartition $S(\mathbf{r})$ of the reflectors for a mean frequency (the center frequency) and for a mean angle of presentation:

$$S(\mathbf{r}) = \int H(\mathbf{k})\, e^{2i\pi \mathbf{k}.\mathbf{r}}\, d\mathbf{k}. \tag{2}$$

When a target is illuminated by a broad-band signal and/or for a large angular extent, it is realistic to consider that the amplitude spatial repartition $S(\mathbf{r})$ of the reflectors depends on frequency f and on aspect angle θ. This repartition depending on the wave vector $\mathbf{k}$, it will be noted in the following by $S(\mathbf{r}, \mathbf{k})$.

2.2. Extended Radar Imaging Based on the Continuous Wavelet Transform

2.2.1. Construction of the Hyperimages

Let $\phi(\mathbf{k})$ be a mother wavelet supposed to represent the signal reflected by a reference target. This target is supposed located around $\mathbf{r} = \mathbf{0}$ and backscatters the energy in the direction $\theta = 0$ and at the frequency f given by $k = \frac{2f}{c} = 1$. A family of function is built $\Psi_{\mathbf{r}_0,\mathbf{k}_0}$ from $\phi(\mathbf{k})$ by the similarity group S [3], [4]:

$$\Psi_{\mathbf{r}_o,\mathbf{k}_o}(\mathbf{k}) = \frac{1}{k_o}\, e^{-j2\pi \mathbf{k}.\mathbf{r}_o}\, \phi\left(\frac{k}{k_o}, \theta - \theta_o\right). \tag{3}$$

The wavelet coefficient $C_H(\mathbf{r}_o, \mathbf{k}_o)$ is defined as the scalar product $C_H(\mathbf{r}_o, \mathbf{k}_o) =< H, \Psi_{\mathbf{r}_o,\mathbf{k}_o} >$ between the complex backscattering coefficient H and the wavelet $\Psi_{\mathrm{r_o},\mathrm{k_o}}$. This scalar product is

defined following [8]:

$$C_H(\mathbf{r}_o, \mathbf{k}_o) = \int_0^{2\pi} d\theta \int_0^{+\infty} k\, H(k,\theta)\, \frac{1}{k_o} \\ e^{j2\pi \mathbf{k}.\mathbf{r}_o} \phi^* \left(\frac{k}{k_o}, \theta - \theta_o \right) dk \quad (4)$$

So we define in the following the hyperImage $S_H(\mathbf{r}, \mathbf{k})$ as the wavelet coefficients $C_H(\mathbf{r}, \mathbf{k})$.

2.2.2. *Properties*

The continuous wavelet transform has three interesting properties. It is possible to build the complex backscattering coefficient $H(\mathbf{k})$ from the wavelet coefficient $C_H(\mathbf{r}_o, \mathbf{k}_o)$:

$$H(\mathbf{k}) = \frac{1}{K_\phi} \int_S d\mathbf{r}_o \int C_H(\mathbf{r}_o, \mathbf{k}_o)\, \Psi_{\mathbf{r}_o, \mathbf{k}_o}(\mathbf{k})\, d\mathbf{k}_o \quad (5)$$

where K_ϕ is defined as the *admissibility coefficient* of the mother wavelet which has, to build $H(\mathbf{k})$ from the wavelet coefficients, to respect the constraint:

$$K_\phi = \int |\phi(\mathbf{k})|^2 \, \frac{d\mathbf{k}}{k^2} < +\infty \quad (6)$$

The second property is the isometry:

$$\frac{1}{K_\phi} \int_S d\mathbf{r}_o \int |C_H(\mathbf{r}_o, \mathbf{k}_o)|^2 \, d\mathbf{k}_o = \|H\|^2 \quad (7)$$

The continuous wavelet transform has interesting properties (reconstruction, isometry, physical interpretation). The principle of the extended radar imaging is based on a physical group of transformations, the similarity group $\mathcal{S}$ that acts on the physical variables $\mathbf{r}$ and $\mathbf{k}$ through rotations $[\mathbf{R}]_\alpha$, dilations a in length (or time) and translations $\delta\mathbf{r}$ as:

$$\begin{array}{ccc} \mathbf{r} & \longrightarrow & \mathbf{r}' = a\,[\mathbf{R}]_\alpha\, \mathbf{r} + \delta\mathbf{r} \\ \downarrow & & \downarrow \\ \mathbf{k} & \longrightarrow & \mathbf{k}' = a^{-1}\,[\mathbf{R}]_\alpha\, \mathbf{k}\,. \end{array} \quad (8)$$

The transformation law of the reflected signal $H(\mathbf{k})$ and its extended image $\tilde{S}(\mathbf{r}, \mathbf{k})$ is therefore given by:

$$\begin{array}{ccc} H(\mathbf{k}) & \longrightarrow & H'(\mathbf{k}) = a\, \exp(-2i\pi \mathbf{k}\cdot\delta\mathbf{r})\, H(a[\mathbf{R}]_\alpha^{-1}\, \mathbf{k}) \\ \downarrow & & \downarrow \\ \tilde{S}(\mathbf{r}, \mathbf{k}) & \longrightarrow & \tilde{S}'(\mathbf{r}, \mathbf{k}) = \tilde{S}(a^{-1}\,[\mathbf{R}]_\alpha^{-1}\,(\mathbf{r} - \delta\mathbf{r}), a\,[\mathbf{R}]_\alpha^{-1}\,\mathbf{k})\,. \end{array} \quad (9)$$

So, in radar imaging, the change of reference coordinates usually is an origin change (translations $\delta\mathbf{r}$), the orientation of axis change (rotations $[\mathbf{R}]_\alpha$), and a scale change (dilations a in length (or time)). For two different observers $\mathcal{A}$ and $\mathcal{B}$ connected by the transformation law (8) ($\mathbf{r}$ is the coordinates of $\mathcal{A}$ and $\mathbf{r}'$ is the coordinates of $\mathcal{B}$), the coordinates of the wave vector are achieved according to (8). $H(\mathbf{k})$ is the backscattering coefficient measured by $\mathcal{A}$ and $H'(\mathbf{k})$ is the backscattering coefficient measured by $\mathcal{B}$, these two coefficients are connected by the law (9). To respect the covariance law, the extended image has to respect the diagram (9).

The multi-dimensional continuous wavelet respects the relation (9). It is not the case for the Cohen class whose the short time fourier transform is a tool. So, to build hyperimage, the multi-dimensional continuous wavelet is selected.

3. POLARIMETRIC TIME-FREQUENCY SIGNATURES

A full polarimetric radar is generally designed to transmit and receive microwave radiations horizontally (h) or vertically (v) polarized. The polarimetric generalization of the scattering coefficient is called the scattering matrix $[\mathbf{S}]$ or Sinclair matrix:

$$[\mathbf{S}] = \begin{bmatrix} S_{hh} & S_{hv} \\ S_{vh} & S_{vv} \end{bmatrix}. \quad (10)$$

The wavelet transform is applied on each of the four polarimetric channels. The resulting Sinclair scattering matrix now depends on the frequency and on the illumination angle and is called hyper-scattering matrix:

$$[\mathbf{S}](\mathbf{r}, \mathbf{k}) = \begin{bmatrix} S_{hh}(\mathbf{r}, \mathbf{k}) & S_{hv}(\mathbf{r}, \mathbf{k}) \\ S_{vh}(\mathbf{r}, \mathbf{k}) & S_{vv}(\mathbf{r}, \mathbf{k}) \end{bmatrix}. \quad (11)$$

By applying the polarimetric coherent decompositions to the hyper-scattering matrix, we obtain, on one hand, a polarimetric evolution of the scatterers versus emitted frequency and observation angle, on the over hand a polarimetric spatial response for each frequency and angle of illumination. This defines the polarimetric hyperimage concept [6] (see Fig. 1).

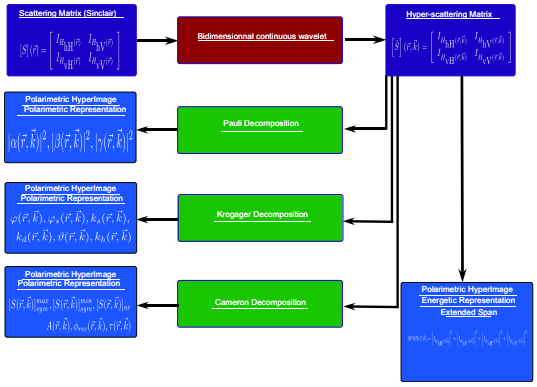

Fig. 1. Algorithm process to obtain polarimetric hyperimages

All in all, for each reflector located at $\mathbf{r}_0 = (x_0, y_0)^T$, we can extract its feature $\tilde{I}(x_0, y_0, f, \theta)$ for each frequency f and for each angle θ. This aspect is the one we have decided to point out in order to see if this quantity can be interpretable in terms of target characteristics. This signature is called polarimetric time-frequency signature.

4. SUPERVISED CLASSIFICATION

Neural networks are non-linear statistical data modeling tools. They can be used to find pattern data [9].

4.1. Multi-Layer Perceptron

A multi-layer perceptron is a feedforward artificial neural network model that maps sets of input data onto a set of appropriate output. The structure of our multi-layer perceptron is described figure (2). It is composed of nodes whose the processing is [10]:

$$a_j^{(1)} = \sum_{i=1}^{d} w_{ij}^{(1)} x_i + b_j^{(1)} \quad (12)$$

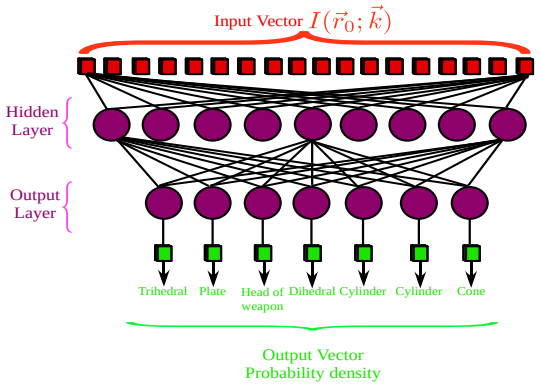

Fig. 2. Architecture of the multi-layer perceptron

Where $a_j^{(1)}$ associated input with each hidden unit. Here $w_{ij}^{(1)}$ represents the elements of the first-layer weight matrix and b_j are the bias parameters associated with the hidden unit. The variables $a_j^{(1)}$ are then transformed by the non-linear activation function of the hidden layer. The activation function is $\tanh(.)$. The outputs of the hidden units are given by $z_j = \tanh(a_j^{(1)})$ which has the property:

$$\frac{dz_j}{da_j^{(1)}} = 1 - z_j^2$$

The z_j are then transformed by the second layer of weights and biases to give second-layer activation values $a_k^{(2)}$:

$$a_k^{(2)} = \sum_{j=1}^{M} w_{ij}^{(2)} z_j + b_k^{(2)} \tag{13}$$

Finally, these values are passed through the output-unit activation function to give output values y_k. For the more usual kind of classification problem in which we have of c mutually exclusive classes, we use the *softmax* activation function of the form [10]:

$$y_k = \frac{\exp(a_k^{(2)})}{\sum_{k'} a_{k'}^{(2)}} \tag{14}$$

Our multi-layer perceptron is a three layers with a number of nodes of the input layer equal to the number of input. The output layer is equal to the number of class to obtain a probability density whose the maximum defines the class which the scatterer belongs to. The number of nodes of the hidden-layer is calculated by: $N = \sqrt{N_{input} N_{output}}$.

4.2. Learning Basis

In supervised learning, a set of known signatures is given and the aim is to find a function in the allowed class of functions that matches the examples. The cost function is related to the mismatch between the mapping and the data and it implicitly contains prior knowledge about the pattern recognition problem.

Our learning basis is made up seven targets: a trihedral, a head of weapon, a plate, a dihedral, a cylinder, another cylinder with different curvature and a cone. The backscattering coefficient of the targets (1) is measured for a frequency band between $[12, 18]$ GHz with a sampling step 25 MHz and an angular excursion from $-20\,\mathrm{deg}$ to $20\,\mathrm{deg}$ with a sampling step $1\,\mathrm{deg}$. Then, the image full-resolution is built according to (2). All in all, the polarimetric time-frequency signatures of manually selected scatterers are extracted as explained in the former part.

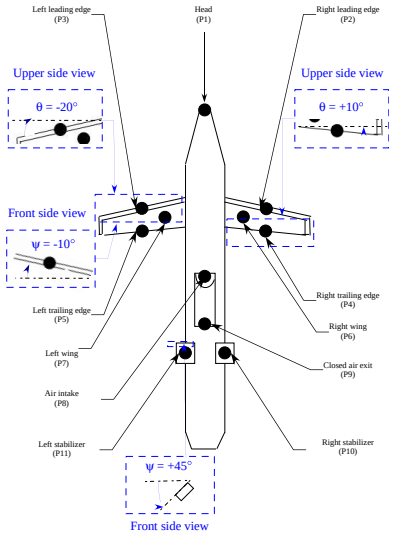

Fig. 3. Diagram of the "Cyrano" weapon model

These signatures are valid for an aspect angle centered on $0\,\mathrm{deg}$ and for a scale of the targets. To release the orientation phenomena and the different scale, it must be taken to notice the covariance law. A rotation is equivalent to an angular translation in the time-frequency plane. So the former signatures are translated and completed with a zero-padding that generates our learning basis for each target. For the scale problem, we make the assumption that the scale of the target under study is the same of the learning basis targets. Of course, it is not realistic however the contraction and dilation on frequency are not the most important phenomena.

5. CLASSIFICATION RESULTS

The target under study is a "Cyrano" weapon model in steel described in Fig. 3. The backscattering coefficient (1) of the target is measured for a frequency band between $[12; 18]$ GHz with a sampling rate 7.5 MHz and an angular excursion from $-20\,\mathrm{deg}$ to $20\,\mathrm{deg}$ with a sampling rate $0.5\,\mathrm{deg}$. Then, the image full-resolution is built according to (2). On this image, the leading edges does not respond because their backscattering behavior is centered on $\pm 20\,\mathrm{deg}$. Then, the polarimetric time-frequency signatures of scatterers are extracted as explained in the former part. All in all, these signatures are sent to the neural networks.

The choice of the mother wavelet has a Gaussian shape. Its bandwidth, determined by the experimentation, has been set to $1/6$th of total frequency bandwidth that represents the best compromise of resolution between space and frequency.

5.1. Extended Span Results

The results of classification based on the extended span polarimetric time-frequency signatures are represented on the figure (4). The

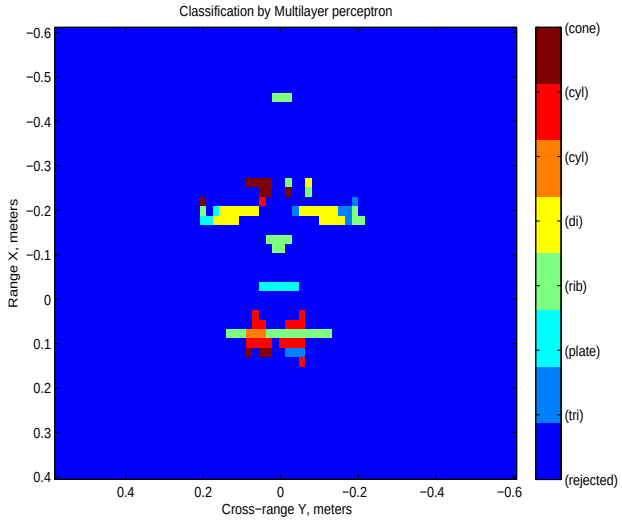

Fig. 4. Classification obtained by the extended span polarimetric time-frequency signatures

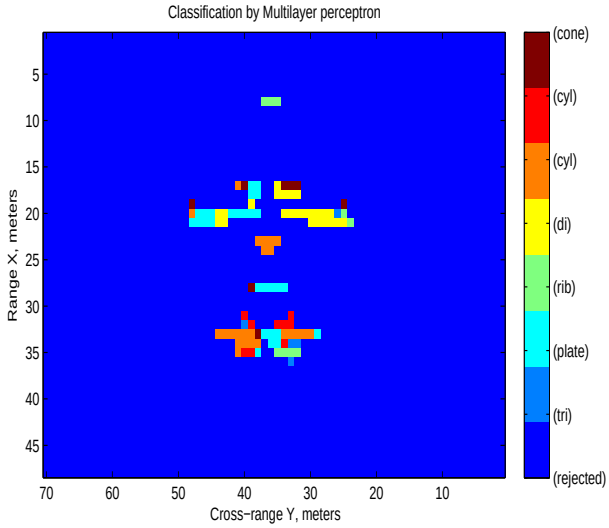

Fig. 5. Classification obtained by the Pauli polarimetric time-frequency signatures

head of "Cyrano" is classified as a head of weapon. The trailing edges of wing are identified as dihedral. It can be explained by the fact that the responses of the edges and of diplane are directive responses. The closed air exit is classified as a specular plate because the response is directive. The open air intake is identified as a head of weapon because the polarimetric time-frequency signature is isotropic and non-dispersive. For the stabilizers the classification is a melting pot of cylinder, head of weapon and cone contribution.

5.2. Pauli Time-Frequency Results

The results of the Pauli hyperimage classification are described on the figure (5). The head of "Cyrano" is classified as a head of weapon. The trailing edges of wing are identified as dihedral or plate. It can be explained by the fact the responses of the edges are directive responses with a melting pot of simple bounce and double bounce contributions. However, the symmetry of the "Cyrano" geometry is not found again that is difficult to explain. The closed air exit is classified as a specular plate because the response is a directive reflection. The open air intake is identified as a cylinder because the polarimetric time-frequency signature is isotropic and non-dispersive. For the stabilizers the classification is a melting pot of cylinder, head of weapon and plate.

6. CONCLUSION

The polarimetric hyperimages allow to extract polarimetric time-frequency signatures. These signatures characterize scatterers and a supervised classification highlights this point of view. Future work will consist in improving the learning basis and in using it to classify scatterers on SAR images.

7. REFERENCES

[1] M. Soumekh, *Fourier Array Imaging*. Englewood Cliffs: Prentice Hall, 1994.

[2] ——, *Synthetic Aperture Radar Signal Processing : with MATLAB Algorithms*. New York: John Wiley and Sons, 1999.

[3] J. Bertrand and P. Bertrand, "The concept of hyperimage in wide-band radar imaging," *IEEE Trans. Geosci. Remote Sensing*, vol. 34, no. 5, pp. 1144–1150, Sep. 1996.

[4] J. P. Ovarlez, L. Vignaud, J. C. Castelli, M. Tria, and M. Benidir, "Analysis of sar images by multidimensional wavelet transform," *IEE Proc. Radar. Sonar. Navig.*, vol. 150, no. 4, pp. 234–241, Aug. 2003.

[5] M. Tria, J. P. Ovarlez, L. Vignaud, J. C. Castelli, and M. Benidir, "Discriminating real objects in radar imaging by exploiting the squared modulus of the continuous wavelet transform," *IEE Proc. Radar. Sonar. Navig.*, vol. 1, no. 1, pp. 27–37, Feb. 2007.

[6] M. Duquenoy, J. Ovarlez, L. Ferro-Famil, L. Vignaud, and E. Pottier, "Study of dispersive and anisotropic scatterers behavior in radar imaging using time-frequency analysis and polarimetric coherent decomposition," in *Proc. IEEE radar conference*, Verona,USA, Apr. 24–27, 2006, pp. 180–185.

[7] D. Mensa, *High Resolution Radar Imaging*. USA: Artech House, 1981.

[8] M. Tria, "Imagerie radar à synthése d'ouverture par analyse en ondelettes continues multidimensionnelles," Ph.D. dissertation, Univ. of Paris-Sud, Paris, France, Nov. 2005.

[9] B. Ripley, *Pattern Recognition and neural networks*. Oxford, 1995.

[10] I. Nabney, *Netlab : Algorithms for pattern recognition*. Springer, 2002.